Progress in Organic Coatings 189 (2024) 108218

Contents lists available at ScienceDirect

Progress in Organic Coatings

journal homepage: www.elsevier.com/locate/porgcoat

Intensified metallic effect and improved tribocorrosion resistance through microwave-based fabrication of metallic powder coatings

Wei Liu [a], Marshall Yang [b,d], Xinping Zhu [a,c], Yufu Wei [c], Yolanda Hedberg [b,d,e], Hui Zhang [a,*], Jesse Zhu [a,*]

[a] Department of Chemical and Biochemical Engineering, Western University, N6A 5B9 London, ON, Canada
[b] Department of Chemistry, Western University, N6A 3K7 London, ON, Canada
[c] Wesdon River Powder Paint Scientific Research Co., Ltd, 528000 Foshan, Guangdong, China
[d] Carbon to Metal Coating Institute (C2MCI), Queen's University, K7L 3N6 Kingston, ON, Canada
[e] Surface Science Western, Western University, N6G 0J3 London, ON, Canada

ARTICLE INFO

Keywords:
Interface
Surface
Corrosion
Wear

ABSTRACT

In this paper, metallic powder coatings (MPC) were investigated as base powder coatings incorporating metallic flakes, providing finishes with a sparkly metallic effect. While MPC offers environmental advantages over liquid coatings by eliminating the usage of solvents, it presents challenges in achieving an intensified and stable metallic effect required by high-end products. This is primarily due to the limitations of the friction-based bonding technique, such as non-selective heating, employed in the current commercial production of MPC. To address this challenge, a microwave-based bonding method was developed that utilizes microwave energy as the heating source instead of stirring friction. This innovative approach leverages the selective heating properties of microwaves to produce qualified MPCs suitable for high-end products. Compared to the current friction-based method with a heating rate of approximately 4 °C/min, microwave heating achieved a significantly faster heating rate of approximately 16 °C/min, owing to the interface polarization effect. The microwave heating engendered a heightened efficacy in forging bonds between coating particles and Al flakes. As a consequence, in scenarios where equal weight percent of Al flakes was introduced, the microwave-treated specimens evinced a stronger metallic effect and enhanced stability compared to friction-heated ones. Furthermore, three-dimensional images of the Al flakes in the coating confirmed that microwave-heated films manifested an elevated flip-flop effect. Tribocorrosion test outcomes underscored that microwave-heated films exhibited higher open circuit potentials (OCP), indicating superior corrosion resistance, alongside better wear resistance compared to friction-heated ones. The microwave-based method obtained stronger and more stable MPCs with better corrosion and wear resistance, showing the promising potential for the expansion of MPC applications into the domain of high-end commodities.

1. Introduction

Functional polymer coatings (FPC) have been heavily applied in many fields [1–4]. Metallic powder coating, as one important member of FPC, finds widespread application in various industries, including automotive, appliance, construction, electrical, petrochemical, shipping, aerospace, and hardware [5–7]. These coatings typically consist of base coating particles combined with metal flakes such as aluminum, copper, and nickel [8]. One notable characteristic of metallic powder coatings (MPC) is the incorporation of metal flakes, which imparts a sparkly effect and yields a surface resembling metal. This surface also exhibits a flip-flop effect, where the amount of reflected light varies with the viewing angle due to differences in flake size, reflectivity, and orientation within the coating [9]. In addition, the inclusion of metal flakes provides enhanced wear and corrosion resistance to the underlying substrates [7,10–12]. MPCs can be categorized into three types based on their base coatings: oil-borne, water-borne, and powder coating [13,14]. Since growing environmental concerns, the usage of oil-borne coatings, which contain up to 60 wt% organic solvents, has been progressively restricted by regulatory bodies [15–17]. Although

---

* Corresponding authors at: Department of Chemical and Biochemical Engineering, Western University, N6A 5B9 London, ON, Canada.
E-mail addresses: hzhang1@uwo.ca (H. Zhang), jzhu@uwo.ca (J. Zhu).

https://doi.org/10.1016/j.porgcoat.2024.108218
Received 12 October 2023; Received in revised form 22 December 2023; Accepted 2 January 2024

water-borne coatings are less detrimental to the environment, they still contain a small amount of (generally around 5 wt%) organic solvents, such as glycol ethers and alcohols, resulting in volatile organic compounds (VOCs) emissions during film formation [18]. In contrast, powder coating involves the application of 100 %-solid, free-flowing powder (30–50 μm) onto a substrate without the need for organic solvents. Consequently, it offers VOC-free emissions and represents an environmentally friendly alternative to the other two coating types [19,20]. This work aims to establish an improved production method for powder-coating MPCs.

Although the exclusion of solvents provides an environmental advantage, it presents a new challenge in ensuring that the collected and original powders have a similar metal flake content [21]. When MPCs are applied using electrostatic spray systems with pressured air, there are typically undeposited powders, about 10–40 wt%, that must be collected and reclaimed to reduce costs and minimize chemical waste [22]. Fig. 1a illustrates that after electrostatic spraying and collecting, the contents of metal flakes in the collected and original powders differ when the two components are not bonded. This disparity arises from distinct differences in shape, density, dielectric properties, and conductivity between the metal flakes and base coating particles. Consequently, the collected powders cannot be reclaimed to obtain a qualified MPC with no apparent change in the metallic effect. Conversely, achieving a strong bond between the two components significantly reduces the disparities in properties, enabling the metal flake content in the collected and original powders to become more closely aligned. As a result, the collected powder can be reclaimed to the original powder and re-sprayed onto substrates, achieving a stable metallic effect (see Fig. 1b).

The current bonding technology of MPCs employs friction (high-speed stirring) and/or water jackets as heat sources to soften the resinous part of the base coating particle and make its surface sticky, which allows metal flakes to adhere and bond [12]. According to the bonding mechanism, it is obvious that the less the content of the metal flake, the easier the bonding process. To secure a stable metallic effect, the content of metal flakes of this technology is usually less than 2.5 wt% due to its several inherent issues [5]. The first and most significant issue is low heating efficiency and non-uniform temperature distribution of friction or water-jacket heating. The second one is the severe bending or grinding of metal flakes during high-speed stirring, which reduces the intensity of the metallic effect. The low content (≤2.5 wt%) and bending/grinding of metal flakes, meaning a weak metallic effect and less protection, restrict the MPC application to high-end products which require stable and intensified metallic effects [23,24]. Hence, a vast paint market is untapped and a new bonding approach for MPCs that can solve the above issues is imperative.

Various efforts have been made to prepare MPCs with high and stable metallic effects in recent years. Gunde et al. demonstrated that adjusting the bonding time and temperature could enhance the metallic effect consistency based on the present bonding technology [5]. Other researchers have proposed the modification of metal flake surfaces with adhesive materials to improve the stability of metallic effects, such as acrylic acid [25], polyethylene wax [26], C6-C8 fatty acids [27], and polyacrylic acid [12]. However, these methods are all based on the current bonding method (friction heating) and decrease the metallic effect to some degree due to surface modification and the remained issues mentioned earlier, which restrict their industrial applications. In contrast to friction and water-jacket heating that mainly transfer heat through surfaces, microwave heating brings various benefits through dielectric heating, including efficiency, ease of control, safety and cleanliness [28,29]. As a result, microwave heating finds successful application across diverse industrial sectors, including cooking, sterilization, drying, and medical treatments [30–33]. Microwave radiation generates heat energy within the material when the molecules attempt to align with the alternating electromagnetic field and experience friction as they constantly reorient themselves [34]. Applying microwave heating in metallic powder coating inherently brings these advantages into this new area. Most importantly, Metaxas and Meredith pointed out that adding metal particles into nonmetals, in some cases, can lead to a higher microwave absorption because of the polarization at the interface of the nonmetal and metal under the microwave electromagnetic field [35]. According to this theory, a higher temperature is expected at the contact area of the base coating particle (nonmetal) and metal flake (metal), which is exactly desired in the heat-bonding process of MPCs.

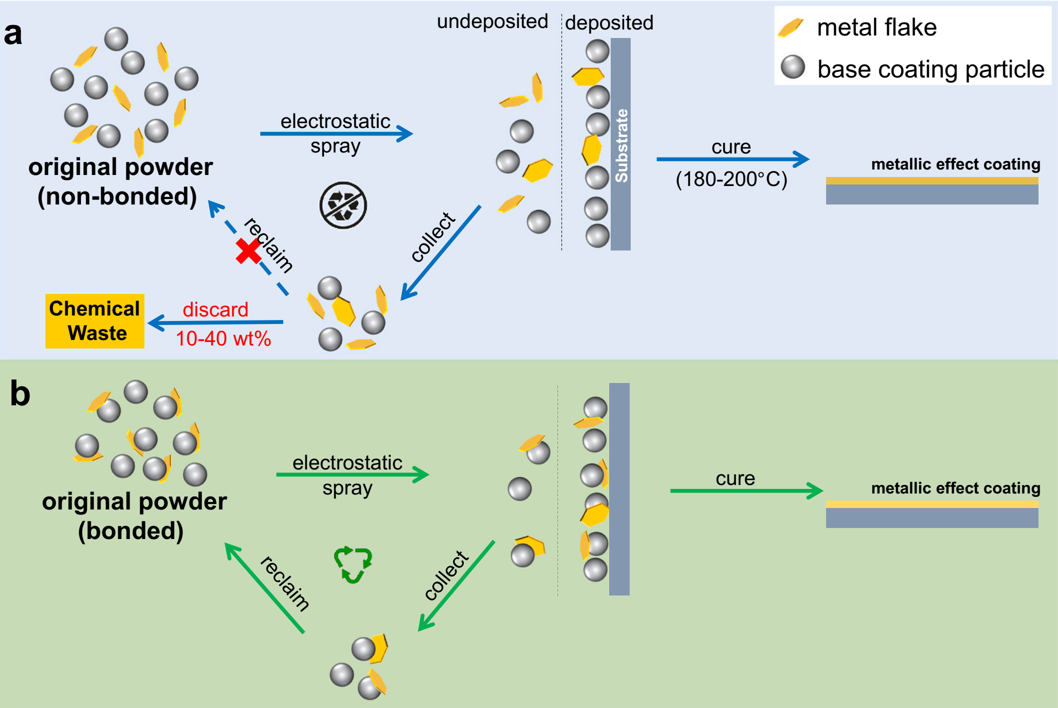

Fig. 1. Schematic of the difference between (a) non-bonded and (b) bonded MPCs sprayed by an electrostatic system.

Despite the potential benefits, no study has explored the utilization of microwave energy to produce MPCs with a metal flake content exceeding 2.5 wt% [36].

This research aims to address the current issues by applying a pioneering approach using 2.45 GHz microwave to produce MPCs, which could potentially overcome the limitations associated with current technologies. In pursuit of this objective, a self-designed microwave heating device was constructed to facilitate the heating and bonding of MPCs. Subsequently, a comprehensive analysis and discussion of the experimental results were conducted regarding the metallic effect and tribocorrosion behaviors of samples prepared through friction (current method) and microwave heating. Tribocorrosion is the concomitant action of chemical/electrochemical corrosion and mechanical wear processes [37]. The findings of this study provide valuable insights into the production of MPCs with superior anti-corrosion characteristics and a stable, intensified metallic effect.

2. Experimental

2.1. Materials

High gloss polyester powder paint (bright white, HS144814) from Huajiang Powder Coating Co. (Guangdong, China) was chosen as the base powder coating. Aluminum flakes (ZPC 330, with a stearic acid-treated surface) from Zuxing New Material Co., Ltd. (Shenzhen, China) were used as laminar metallic pigments. Al panels (15 cm by 7.6 cm) from Q-Lab Co. (OH, USA) were utilized as substrates for coating films. Sodium hydroxide from Fisher Scientific Co., Ltd. (MA, USA) served as a reacting agent for gas-volumetric analysis for aluminum (Al) content analysis. Hydrochloric Acid (HCl), sodium hydroxide (NaOH) and methyl ethyl ketone (MEK) from Fisher Scientific (MA, USA) were used for analyzing the properties of films.

2.2. Preparation of microwave-heated powders and coated samples

The untreated powders (base powder coating and aluminum flakes) with low and high Al flake contents were prepared by mixing, whose contents of Al flake were 2.33 wt% and 4.94 wt%, respectively. As seen in Fig. 2, the control samples, which were manufactured by Huajiang Powder Coating Co. from the above-untreated powders using a conventional bonding machine (SHTBD10, Sun-Hitech Technology Ltd., Xiamen, China), were bonded by friction-based bonding (FB) method with a high-speed stirring of 900 rpm at 62°C, followed by sifting, electrostatic spraying and curing to obtain the metallic powder coating films. In preparation of the microwave-bonded samples, microwave energy was employed as a heat source to replace friction and/or water jacket heating. The microwave heating machine was self-built as given in Fig. S1. The microwave heating rates of prepared powders were recorded by the two thermocouples equipped with the device.

In detail, the microwave-bonded powder samples were prepared following these steps: a) load the untreated powder (10 kg) into the chamber; b) heat the loaded powder with nine microwave transmitters at a stirring speed of 500 rpm to the set temperature shown in Table 1; c) maintain this temperature at a stirring speed of 800 rpm for 120 s; d) discharge the loaded powder to a quenching container for cooling down to room temperature; e) sift the discharged powder by a 120 mesh screen.

Table 1 shows the information of the prepared samples. For the original powders, the contents of Al flake (Al contents) were 2.33 (low) and 4.94 (high) wt%, respectively. After optimization of temperature, four powder samples were prepared in this paper.

The deposited powders and final films were prepared by the below steps: a) spray a powder sample onto two substrates at each voltage (30, 60 and 90 kV) with the air supply unchanged (6.5 m^3h^{-1}) by an electrostatic automatic spraying system and a corona gun (Gema Switzerland GmbH, St. Gallen, Switzerland); b) scrap off the deposited powder from one of the two substrates for Al content analysis; c) cure (190°C, 10 min) the deposited powder on the other substrate into a film for metallic effect and tribocorrosion characterizations. Each step was repeated three times.

2.3. Simulation of microwave heating of MPC

A 2D model of COMSOL for simulating the microwave heating processes of MPC was built for calculating the distribution of the electric field in the steady-state frequency domain by electromagnetic analysis. Afterward, transient electromagnetic heating and heat transfer in solids (base coating with Al flakes) were coupled and simulated based on the electric field to showcase how heat is redistributed between the two materials.

Maxwell's equations were solved to determine electric field distribution in the microwave cavity as follows,

$$\nabla \times \mu_r^{-1}(\nabla \times E) - k_0^2\left(\varepsilon_r - \frac{j\sigma}{\omega\varepsilon_0}\right)E = 0 \tag{1}$$

Table 1
Compositions and labels of control and microwave-heated samples.

No.	Base coating (wt%)	Al flake (wt %)	Heating source	Temp. (°C)	Label
1	97.67	2.33 (low)	Friction (commercial)	62	FN-L
2	97.67	2.33	Microwave	59	MW-L
3	95.06	4.94 (high)	Friction	62	FN-H
4	95.06	4.94	Microwave	60	MW-H

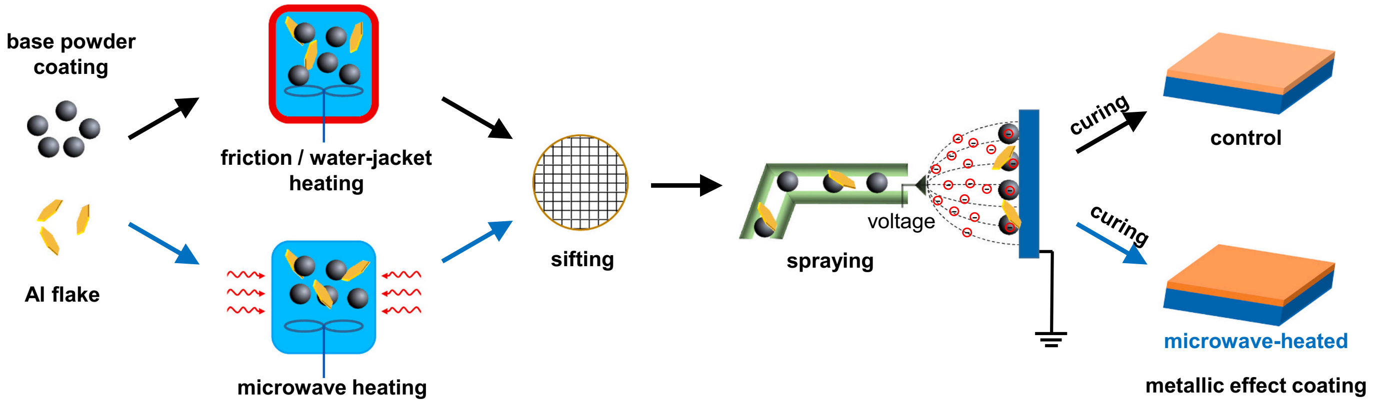

Fig. 2. Preparation processes of MPC by friction-based and microwave-based methods.

where μ_r is the permeability; ε_r is the permittivity of the material; σ is conductivity in S/m; k_0 is wave number in free space; ω is angular frequency in rad/s; E is the strength of electric field in V/m; ε_0 is the permittivity of vacuum. Eq. (1) can be accessed from the Electromagnetic Waves, Frequency Domain interface of COMSOL.

The heat transfer equation that couples with microwave field can be referred by Eq. (2). The surface current density (J_{s0}, A/m^2) was employed to simulate the interface polarization between the base coating and Al flake according to Eq. (3).

$$\rho \ C_p \ \frac{\partial T}{\partial t} + \rho \ C_p \ \mathbf{u} \cdot \nabla T = \nabla \cdot (k \ \nabla T) + Q_e \tag{2}$$

$$\mathbf{n} \times (H_1 - H_2) = J_{s0} \tag{3}$$

where ρ is material density in kg/m^3; C_p is specific heat in J/(kg K); k is thermal conductivity (W/mK), T is temperature (K), u is velocity vector (m/s); Q_e is the volumetric heat generation due to the incident microwave energy (W/m^3); $\mathbf{n}$ represents the normal vector to the surface; H_1 and H_2 are two different values of magnetic field intensity at the surface (A/m).

The transit solid-solid heat transfer between the base coating and Al flake was obtained by solving the Navier–Stokes equation:

$$\rho \ C_p \ \mathbf{u} \ \nabla T + \nabla \cdot (-k \ \nabla T) = Q + \frac{q_0}{d_z} + Q_{ted} \tag{4}$$

where Q is the heat source from microwave energy (W/m^3), q_0 is the inward heat flux (W/m^2); Q_{ted} is the thermoelastic damping and accounts for thermoelastic effects in solids (W/m^3). All the parameters applied in these simulations can be found in Table S1.

2.4. *Characterization of bonded powders*

To directly analyze the bonding states between the base coating particles and Al flakes, all the powder samples were observed by a scanning electron microscope (SEM, SU3500, Hitachi Ltd., Tokyo, Japan), equipped with an energy dispersive X-ray spectrometer (EDS), after gold-sputtering for 1.5 min. The size distribution of each powder sample was measured three times using a laser diffraction particle size analyzer in D.I. water, the refractive index inputs of powder and D.I. water were 1.55 and 1.33, respectively (LS-POP6, Omec Instruments Ltd., Zhuhai, China). Each sample was measured in triplicate.

As discussed in Section 1, ensuring that the original and deposited powder have close Al content is crucial for a consistent metallic effect. The Al contents of deposited powders mentioned in Section 2.2 were precisely analyzed by a gas-volumetric method based on the following reaction:

$$2Al \ (s) + 2NaOH \ (aq) + 2H_2O(l) = 2NaAlO_2 \ (aq) + 3H_2 \ (g) \tag{5}$$

The Al contents in the powders were calculated by the following equation:

$$\omega = \frac{2 \ V_{H_2} \ M_{Al}}{3 \ V_m \ m_{sa}} \ \times \ 100\% \tag{6}$$

where ω is the Al content (wt%); V_{H_2} is the volume of hydrogen (mL); M_{Al} is the relative atomic mass of aluminum (g/mol); V_m (mL/mol) is the molar volume of hydrogen at 25°C and 1 atm; m_{sa} (g) is the total mass of the powder sample. Each powder was measured by the gas-volumetric method three times. The device for the above analysis is shown in Fig. S2.

During the electrostatic spraying of powder coating, generally 10–40 wt% of powder fails to deposit onto the substrate and will be reclaimed and resprayed as shown in Fig. 1. To calculate the deposited Al content after *N* times of recycling, several assumptions were made based on published work [38,39]: 1) the ratio (Ro) of deposited Al content (ω_{dep}) to original addition (ω_{ori}) is unchanged during recycling; 2) the deposition rate (R_{dep}) is 0.8; 3) respraying rate (R_{respr}) is 0.25. Therefore, the difference ($\Delta\omega^{(N)}$) between deposited Al content after *N*-time recycling and original addition can be calculated:

$$Ro = \frac{\omega_{dep}^{(1)}}{\omega_{ori}} \tag{7}$$

$$\Delta\omega^{(N)} = \left(1 - R_{respr}\right) \ \omega_{ori} \ Ro + R_{respr} \ \omega_{dep}^{(N-1)} \ \frac{1 - R_{dep} \ Ro^2}{1 - R_{dep}} - \omega_{ori} \tag{8}$$

2.5. *Characterization of metallic effect*

To evaluate the reflectance of the surface, the 20° and 60° gloss values of the final film were measured by a 408 triple-angle gloss & DOI meter (Elcometer Limited, Manchester, UK) at six uniformly distributed sites. The surfaces of coatings films were observed under an optical microscope (OM, VHX-950F, Keyence Corporation, Osaka, Japan) to compare the metallic effect directly. ImageJ software further analyzed the area percentage of Al flake on the observed surface (Al area) in the optical images. In addition, the coated panels were cut into pieces and mounted in epoxy to observe the cross-sectional morphology. Then the whole mounting was ground and polished before being characterized by the optical microscope.

To analyze the flip-flop effect, the final coatings were determined using micro-CT (X-ray micro-computed tomography, Zeiss Xradia 410 Versa Micro-CT, Carl Zeiss Microscopy GmbH, Jena, Germany) to obtain a 3D view of the dispersion of Al flakes. Using the 3D images, the orientation distribution of the Al flakes in the coatings was analyzed using Jupyter Notebook (Python 3.0). The acute angle (α) between the Al flakes and the substrate surface was defined as the orientation of the Al flakes. For every ten degrees between 0 and 90, the number of Al flakes with angles within that range was counted and divided by the total number of Al flakes. These percentages illustrate the orientation distribution of the Al flakes in the coatings.

The pencil hardness, adhesion, impact resistance and bending of prepared films were determined according to ASTM D3363, D3359, D2794 and D522 by an Elcometer 501 pencil hardness tester, an Elcometer 107 cross hatch cutter, an Elcometer 1615 variable impact tester and an Elcometer 1510 conical mandrel (Elcometer Limited, Manchester, UK), respectively. The acid (1 M HCl), alkali (1 M NaOH) resistance and hydrolytic stability (100°C) were tested for 1 h based on ASTM D1308. The solvent resistance was evaluated by the MEK-rubbing test (50 double rubs) according to D5402. The thickness of the final films was measured by a thickness meter (Positector 6000, Defeisko Co. NY, USA) at four uniformly distributed sites.

2.6. *Tribocorrosion analysis*

The coated aluminum (Al) panels, with a controlled coating thickness of 50 ± 5 μm, were sectioned into squares measuring 1.8 cm × 1.8 cm before the tribocorrosion testing. These specimens were then immersed in a 3.5 wt% NaCl solution for 10 days at room temperature. The tribocorrosion characterization of the specimens was conducted using an integrated Bruker UMT Tribolab System (Bruker Corporation, Billerica, MA, USA) and Solartron Modulab XM (AMETEK Scientific Instruments, Oak Ridge, TN, USA) electrochemical workstation at room temperature. During the testing, the specimen was secured in the electrochemical clamp cell, with a metal spring contact at the back, whereas the coated front side, with an area of 1.5 cm^2 that was sealed with an O-ring, was exposed to 3.5 wt% NaCl solution. The specimen acted as the working electrode. The reference electrode was an Ag/AgCl reference electrode in a saturated potassium chloride solution. All potentials in the following are expressed against this reference electrode. A ceramic ball with a diameter of 4.4 mm was attached to a carriage and brought into contact with the top surface of the specimen. The motion was a reciprocating, linear ball-on-plate sliding motion. The parameters of the Tribolab system were set as follows: a stroke distance of 1.5 mm, a speed of 1 mm/s, and an applied normal load of 10 N. The tribological and corrosion behaviors of the coating films during friction were evaluated by measuring the open circuit potential (OCP) values and the coefficient of friction (COF) over time. First, the system was allowed to stabilize for 10 min, followed by 30 min of sliding, and another 25 min of no sliding. Each sample was measured three times. Any significant differences ($P \leq 0.05$) were evaluated by comparing two datasets with a *t*-test of unpaired data with unequal variance (KaleidaGraph v. 4.0).

3. Results and discussion

3.1. *Performance of microwave heating*

The efficiency of production is closely tied to the heating performance of microwave or friction methods. A rapid and uniform heating process during the production of MPC can significantly enhance the bonding process between the two components [40]. Fig. 3 illustrates the temperature distribution and heating rate of three powder samples exposed to microwave radiation: A) base coating particles; B) MW-L (2.33 wt% Al flake); C) MW-H (4.94 wt% Al flake). As depicted in Fig. 3d, the heating rate of MPC using friction heating was approximately 4 °C/min. Microwave heating is renowned for its effectiveness and uniformity owing to the principle of dielectric heating. The ability of a material to absorb microwave energy can be mathematically described by the following equation [41]:

$$P = 2\pi f \varepsilon_0 E^2 \ \varepsilon''_{\mathrm{eff}} \tag{9}$$

$$\varepsilon''_{\mathrm{eff}} = \varepsilon''_{\mathrm{e}} + \varepsilon''_{\mathrm{a}} + \varepsilon''_{\mathrm{d}} + \varepsilon''_{\mathrm{if}} \tag{10}$$

where P is the microwave absorbing power per unit volume (W/m^3); f is the frequency of microwave (Hz); E is the electric field intensity (V/m); ε_0 is the permittivity of vacuum; $\varepsilon''_{\mathrm{eff}}$ is the effective dissipation factor of material; $\varepsilon''_{\mathrm{e}}$, $\varepsilon''_{\mathrm{a}}$, $\varepsilon''_{\mathrm{d}}$ and $\varepsilon''_{\mathrm{if}}$ are the electron, atom, dipolar polarization, and interface polarization dissipation factor, respectively. E and f can be regarded as constant in this work, so a larger value of $\varepsilon''_{\mathrm{eff}}$ will lead to greater microwave absorption as well as a higher temperature.

When solely heating the base coating particles (10 kg), the primary mechanism of microwave absorption is dipolar polarization. As depicted in Fig. 3a, the final temperature reaches approximately 32°C after 4 min of microwave radiation. Furthermore, a negligible temperature gradient was observed from the particle's center to its edge, providing evidence that microwave heating occurred from within. However, the heat transferred fast from the inside to the outside considering their small size and relatively high thermal conductivity [42]. The simulated heating rate, approximately 2 °C/min, closely aligns with the experimental data shown in Fig. 3d. The dipolar polarization dissipation factor ($\varepsilon''_{\mathrm{d}}$) of the coating particle can be estimated using the following equation [43]:

$$\varepsilon''_{\mathrm{d}} = \varepsilon' \tan\delta \tag{11}$$

where ε' is the real part of dielectric constant of material; $\tan\delta$ is the loss tangent of material. By using the data from reported research [44,45], the calculated $\varepsilon'_{\mathrm{d}}$ was about 0.017.

When heating the MW-L sample (base coating particles with 2.33 wt % Al flake, 10 kg), the effective dissipation factor primarily arose from the interface and dipolar polarization. Interface polarization occurs at the contacting surfaces of the two materials, while dipolar polarization originated solely from the base coating particles. This is because metals

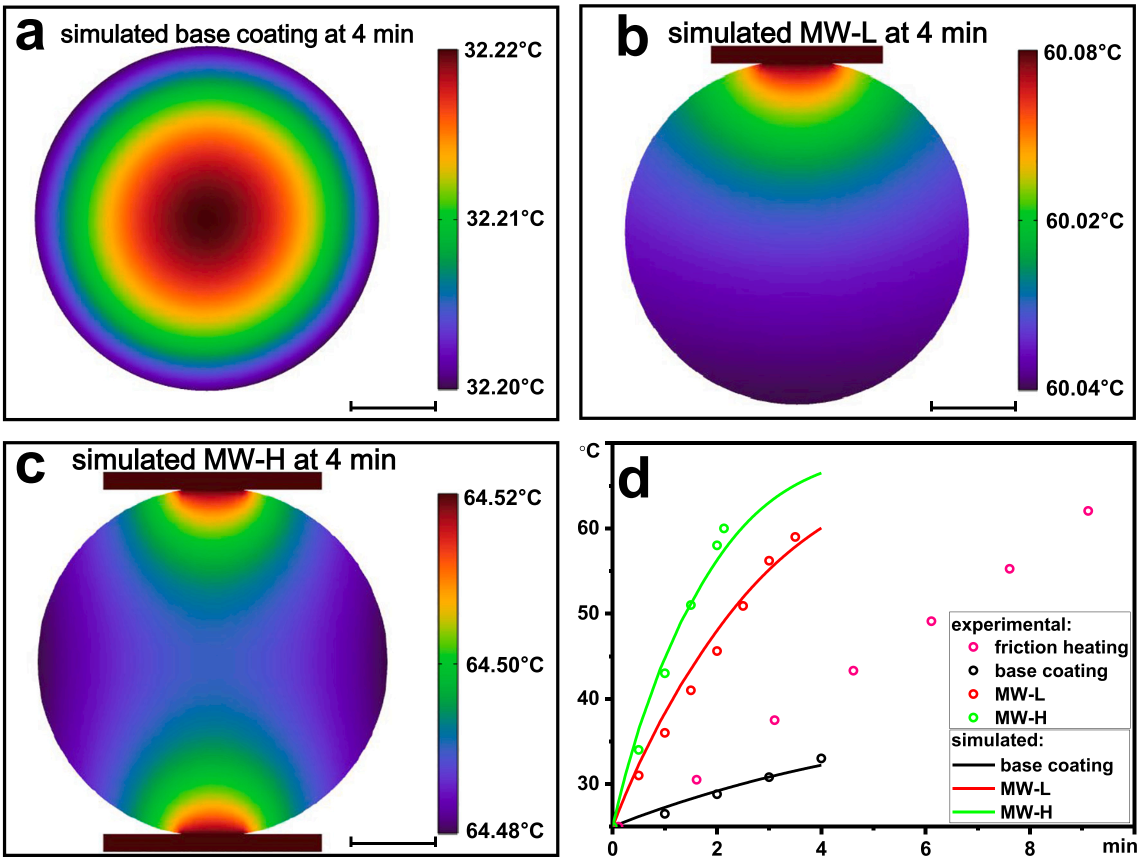

Fig. 3. Simulated and experimental microwave heating rates and temperature distributions: a) base coating particle; b) MW-L; c) MW-H; d) comparison of the microwave and friction heating rates. All the scale bars are 10 μm.

predominantly reflect microwaves rather than absorbing them [35]. As shown in Fig. 3b, the temperature reached 60°C after 4 min of microwave heating, with a relatively higher temperature observed at the interface. The experimental heating rate, as depicted in Fig. 3d, was approximately 11 °C/min. Compared to the results of the base coating particle, there was an increase in the final temperature and heating rate by 28°C and 9 °C/min, respectively. According to Wagner's work, the interface polarization dissipation factor between metal and nonmetal particles can be evaluated by Eq. (12) [46]. Sillars reported that the relaxation time constant can be estimated by Eq. (13) [47].

$$\varepsilon''_{\mathrm{if}} = \frac{9 v \varepsilon'_1 f_{\max}}{1.8 \times 10^{10} \delta_2} \frac{2\pi f \tau}{1 + (2\pi f \tau)^2} \tag{12}$$

$$\tau = \varepsilon_0 \frac{\varepsilon'_1 + \varepsilon'_2}{\delta_1 + \delta_2} \tag{13}$$

where v is the volume fraction of conductive material; $f_{\max}$ in Hz is the frequency of maximum losses; δ is the conductivity in Sm^{-1} of the conductive phase; τ is the relaxation time constant; the subscripts 1 and 2 refer to non-conductive and conductive phase, respectively. After collecting parameters from published articles [36,44,48], $\varepsilon''_{\mathrm{if}}$ is turned out to be around 0.08. Hence, the $\varepsilon''_{\mathrm{eff}}$ for MW-L should be 0.097 according to Eq. (10) which is much higher than that of the base coating particle (0.017).

Remarkably, the heating rate of MW-H displayed in Fig. 3d demonstrated a substantial increase to approximately 16 °C/min as the addition of Al flakes reached 4.94 wt%. This significant enhancement in heating rate can be primarily attributed to the augmented volume fraction of Al flakes. A larger volume fraction (v) results in greater values of $\varepsilon_{\mathrm{if}}{}^{\prime\prime}$ and P (microwave absorption), as described in Eqs. (9) and (12) respectively. This observation suggests that the higher addition of Al flakes corresponded to faster heating rates and reduced processing time. Conversely, in the case of high additions of Al flakes, the friction-based bonding method necessitated an extended processing time to ensure an adequate degree of bonds. Compared to friction heating, the heating rates raised by three times while the bond temperature decreased by about 2°C due to the interface polarization as shown in Fig. 3. Above all, the exceptionally rapid heating rate, achieved through microwave radiation stems from interface polarization, exhibits considerably superior heating efficiency compared to friction-based methods.

The SEM images and EDS mappings of the powder samples after bonding are presented in Fig. 4. The black and white arrows indicate well-bonded and separated Al flakes, respectively. In the EDS mappings, the green and blue patterns represent the presence of Al and Ti elements, respectively. The Ti element was used to identify the position of the base coating particle, as it contains TiO_2 as a white pigment. Since FN-H and MW-H samples contain 4.94 wt% Al flake (Table 1), they exhibited a higher abundance of green patterns than FN-L and MW-L samples. The magnified images of the prepared powders, shown in Fig. S3, clearly display the bonded particles. Noticeably, a greater number of bonded particles was observed in the microwave-heated samples (Fig. 4a and d) compared to the friction-heated samples (Fig. 4a and c), suggesting that microwave heating can facilitate more effective bonding when the amount of added Al flake is the same.

As depicted in Fig. 1, it is crucial for the stability of the metallic effect in coatings that the Al contents of the deposited powders closely match those of the original powders. Gas-volumetric analyses revealed the average Al contents (wt%) of the deposited powders (ω_{dep}) in the FN-L, MW-L, FN-H, and MW-H samples to be 1.29 ± 0.08, 1.87 ± 0.02, 2.89 ± 0.12, and 3.53 ± 0.08, respectively, as presented in Fig. 5a and Table S2. To assess the Al content, each powder sample was sprayed at three different voltages, as the spray voltage affects the ratio when bonding is insufficient. An Al content percentage closer to the original Al content indicates better bonding. Markedly, there is a reduction in deposited Al flake of the prepared samples compared to their original amounts. The reduction could be attributed to the fact that the difference in the ability to capture electrons or anions between Al flakes and base coating particles. The estimation of the maximum charge ($Q_{\max}$) accumulated by a particle passing through an electric field can be determined using the following equation [49]:

$$Q_{max} = 4\pi r_e^2 \varepsilon_0 E \frac{3\varepsilon_r}{\varepsilon_r + 2} \tag{14}$$

where r_e is the equivalent spherical radius; ε_0 is the permittivity of vacuum; E is the electric field strength; ε_r is the relative dielectric con-

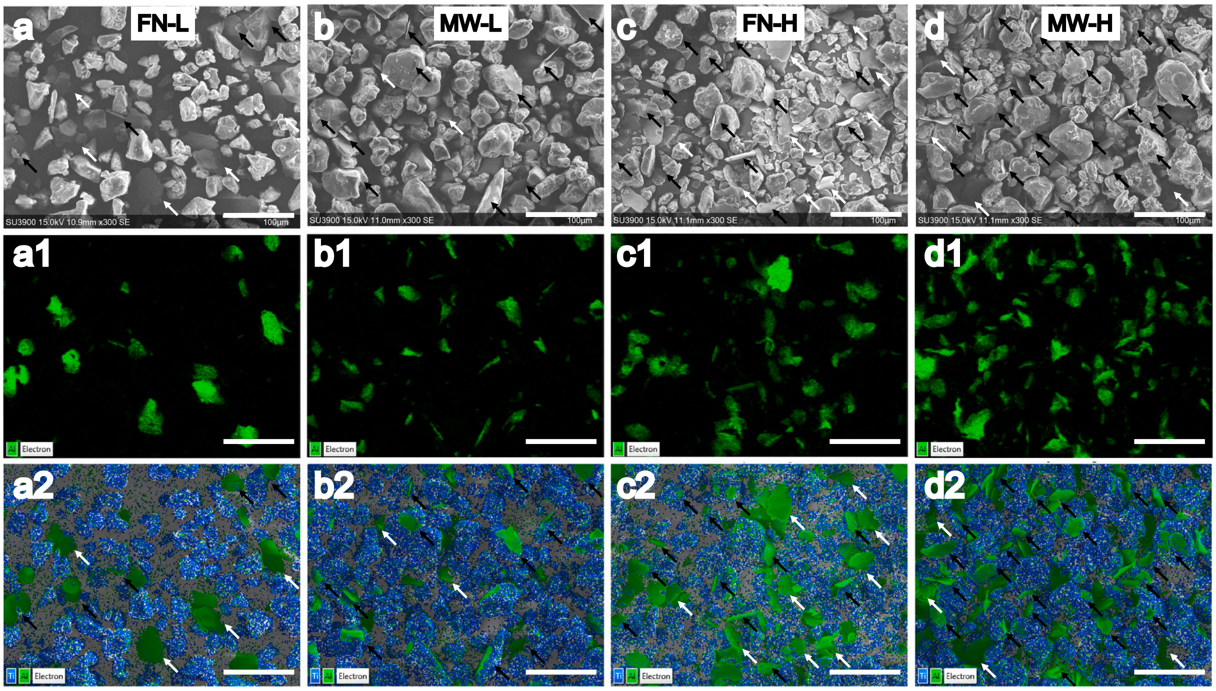

Fig. 4. The SEM and EDS mapping images of friction- and microwave-heated powders with low and high addition of Al flakes. All the scale bars are 100 μm.

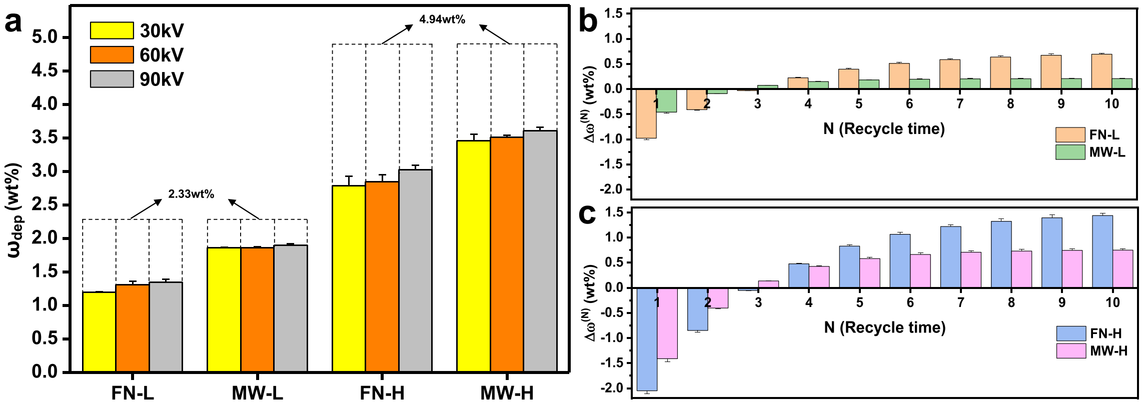

Fig. 5. a) Al contents in the deposited powders sprayed from prepared samples under various voltages; b, c) recycle time vs. the difference between deposited and original Al contents when the original Al content was 2.33 wt% (b) and 4.94 wt% (c).

stant. The average equivalent spherical radius of the used Al flake and base coating particle were approximately 7 ± 0.2 μm and 33 ± 2.3 μm, respectively. Considering published data [50–53], the maximum charge of the base coating particle was about ten times more than that of Al flake. Another reason for the reduction is that the high aspect ratio of Al flake makes it easy to be blown away during spraying. After microwave-based bonding, the ω_{dep} approximately increased by 0.58 wt% when the original Al content (ω_{ori}) was 2.33 wt% and by 0.64 wt% as the ω_{ori} was 4.94 wt%, respectively. Hence, the ω_{dep} of the microwave-heated samples were much closer to the original Al contents. Fig. 5b and c shows the calculated difference (based on Eq. (8)) in Al content between deposited and original powders, $\Delta\omega^{(N)}$, with respect to the recycle time of undeposited powder. The $\Delta\omega$ of the four samples increased from negative to positive values due to the accumulation of Al flake in the undeposited powders. Fig. 5b displays that the $\Delta\omega^{(N)}$ of FN-L ranges from −0.98 wt% to 0.74 wt% with the increase of recycle time, while the range of MW-L narrows to −0.46 wt% to 0.21 wt%. For the high original Al content samples, the range of $\Delta\omega^{(N)}$ narrows from −2.05~1.53 wt% to −1.41~0.76 wt%, respectively. Much narrower ranges of microwave-heated samples in deposited Al contents imply better stability of the metallic effect.

3.2. Metallic and flip-flop effect of coatings

The optical microscope was used to capture top surface and cross-section images of the MPC films, as presented in Fig. 6, aiming to compare their metallic effects. Through direct observation, it is apparent that the presence of Al flakes increased sequentially in the top surfaces (Fig. 6a-d) and cross sections (Fig. 6e-h), with FN-L exhibiting the least, followed by MW-L, FN-H, and finally MW-H. To quantitatively analyze the Al content, Image J was employed, and Fig. 6i illustrates the respective Al areas for the four samples. The Al area percentages in the top surfaces are 12.9 %, 14.8 %, 19.6 %, and 22.3 %, while in the cross sections, they are 2.2 %, 2.8 %, 3.5 %, and 4.3 % for FN-L, MW-L, FN-H, and MW-H, respectively. These findings are consistent with the Al content analysis provided in Fig. 5. Notably, the microwave-heated samples (MW-L and MW-H) exhibited more pronounced metallic effects due to a higher concentration of Al flakes within the film than those prepared via friction heating. The gloss measurements at 20 and 60 degrees for the four coatings are depicted in Fig. 6j. It is observed that the gloss diminishes with increasing Al content in the film. This can be attributed to the fact that there is a greater reflection of light towards non-reflective angles when more Al flakes are present in the final film [6]. In conclusion, both the top surface and cross-section images provide compelling evidence that films prepared using microwave heating exhibit more extensive metallic effects.

MPCs are characterized by their visually appealing and luxurious surfaces, attributed to the flip-flop effect. This effect refers to the phenomenon where the surface reflects varying amounts of light at different angles due to the diverse orientations of aluminum (Al) flakes within the film. In this study, micro-CT imaging was employed to determine the

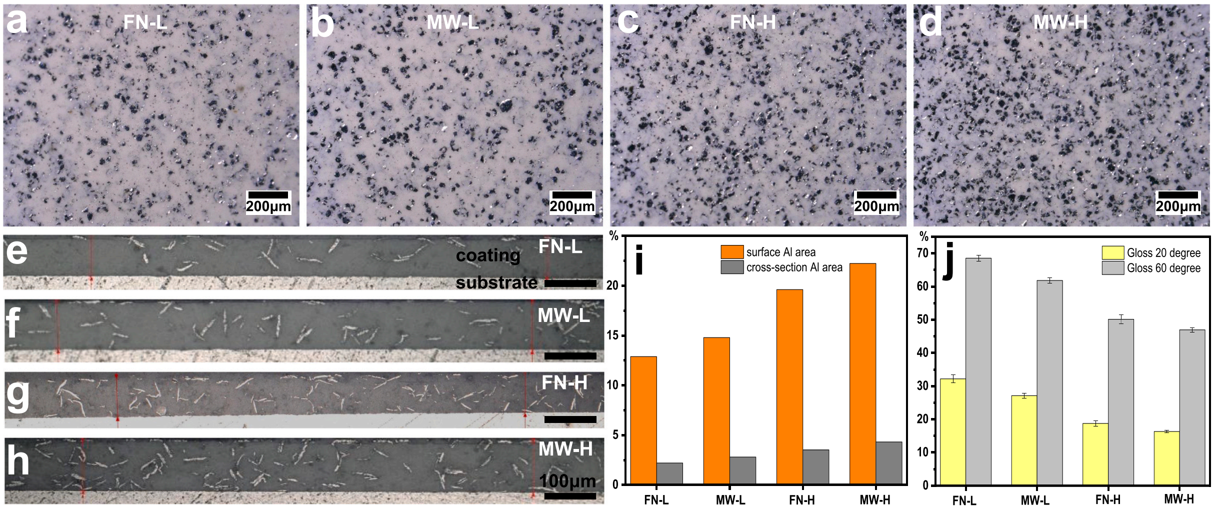

Fig. 6. Al contents in the deposited powders which sprayed from prepared samples under various voltages.

orientation of Al flakes within the film, as depicted in Fig. 7a-d. The Al flakes are represented by green patterns, while the films are indicated by framed cuboids. Fig. S9 provided the top and side views of the 3D images in Fig. 7a-d, with blue and yellow patterns denoting the substrates and Al flakes, respectively. In addition, Fig. 10S exhibited the profiles of films in Fig. 7a-d from surface to near substrate, with the coating and Al flakes represented by black and white, respectively [54]. These images indicate that more Al flakes distribute within the films after microwave heating compared to friction heating. The estimated Al contents of FN-L, FN-H, MW-L, and MW-H based on volumetric pixels from micro-CT data were 1.34, 1.90, 2.69, and 3.58 wt% (Table S3). The observed trend in the quantity of Al flakes across the four coatings matches the results depicted in Fig. 5. Subsequently, the acquired 3D images were analyzed to determine the orientation of each Al flake within the films, as illustrated in the insert of Fig. 7e. The accumulated percentages of Al flakes at different angles in the four films, obtained from the anaconda analyses, are presented in Fig. 7e. In these analyses, a density-based spatial clustering algorithm is applied to cluster the images, calculating the angles between the Al flakes and the horizontal plane [55]. The results in Fig. 7e indicate that during the deposition and curing processes, the Al flakes exhibit a tendency to align parallel to the substrate (angle = 0°). This alignment promotes a larger contact area between the flakes and the substrate or other particles, facilitating more efficient charge transfer [5]. Also, the tension force exerted by resin leveling during the curing process contributes to the parallel alignment of Al flakes with the substrate. Moreover, it was observed that microwave heating facilitates a more uniform distribution of Al flake orientations compared to friction heating. This is mainly because of the increased bonding, which reduces the freedom of orientation during the spraying and curing processes, thereby resulting in a reduced tendency to align with the substrate. In summary, microwave heating enhances the flip-flop effect by reducing the concentration level of Al flake orientations within the coating.

3.3. Tribocorrosion behavior of coatings

The tribocorrosion behavior of the prepared samples was investigated using the open circuit potential (OCP) measurement. OCP provides valuable information about the electrochemical state of the surface [56,57]. If cathodic reaction rates remain constant, a sudden drop of the OCP means a breakdown of the protective surface, whereas an increase in the OCP means that the formation of a surface oxide hinders further anodic reactions (metal oxidation). Fig. 8 depicts the evolution of OCP before, during, and after sliding, along with the coefficient of friction (COF), under a 10 N load in a 3.5 wt% NaCl solution for the four samples. Prior to sliding, the OCP values of FN-L, MW-L, FN-H, and MW-H remained relatively stable around −0.63 V, −0.57 V, −0.52 V, and −0.47 V, respectively. Pure aluminum metal in aerated 3.5 % NaCl solution is expected to exhibit a potential of about −0.8 V (vs. Ag/AgCl) [58,59]. The fact that the initial and final OCP values are higher than that indicates some protection, either because of pre-passivation in the soaking procedure (10 days) or because of the coating. Further, the consistently higher OCP of the microwave-heated samples than the friction-heated ones suggests superior substrate protection. During the initial 5 min of sliding (between 10 and 15 min of the experiment), the OCP values remained relatively constant, while the COF gradually increased due to the minimal damage inflicted upon the three-dimensional interpenetrating network structure of the films during sliding. The increasing COF values resulted from the expanding contact area between the ball tip and the films [60]. Between 15 and 20 min, a drastic OCP drop was observed, as the coating thickness decreased during sliding and the coating disrupted [61,62]. Concurrently, the COF exhibited an increase, reflecting the expansion of the contact area between the ball and the wear track and the change of material in contact as the coating broke down. Remarkably, the OCP values of FN-H and MW-H demonstrated a slower and smaller reduction compared to those of FN-L and MW-L, as the higher Al content in the coating films hindered thickness reduction and provided higher corrosion resistance.

During the remaining duration of sliding (between 20 and 40 min), the OCP values exhibited relative stability because of equilibrium between activation (metal oxidation) and repassivation (reforming of the protective Al_2O_3 surface oxide) processes [61]. The OCP of about −1.1 V (vs. Ag/AgCl) (FN-L) indicates the exposure of bare Al metal (the substrate) to the solution [63]. Consequently, the coefficients of friction (COFs) maintained stable values as follows: FN-L (0.297 ± 0.04), MW-L (0.306 ± 0.05), FN-H (0.323 ± 0.006), and MW-H (0.331 ± 0.004). The higher COF of the coatings with higher Al content resulted from the significantly higher hardness of the Al flakes, producing wear debris and third-body abrasive wear, than that of the polyester matrix [64,65]. Subsequent to the sliding process (40 min onwards), all the OCP values exhibited an increase, indicating the re-passivation of the exposed Al substrate [63].

This finding was corroborated by SEM imaging and EDS mapping of the wear tracks, as shown in Fig. 9. The coating formed adhesive wear in all cases. In Fig. 9a, a1, b, and b1, two coating areas were removed by the sliding, accompanied by cracks on the track of FN-L. The damage resulted in the lowest OCP values during sliding (Fig. 8a). Additionally, Fig. 9a reveals a significant blue area in the 3D image, corresponding to the falloff spot with a track depth of 51 μm. In coating MW-L, no noticeable film falloff was observed, however, approximately ten distinct cracks were present, as shown in Fig. 9c–d. The EDS maps in Fig. 9c1–d1 confirm that these cracks exposed the substrate to the solution. Fig. 10b shows a track depth of approximately 32 μm,

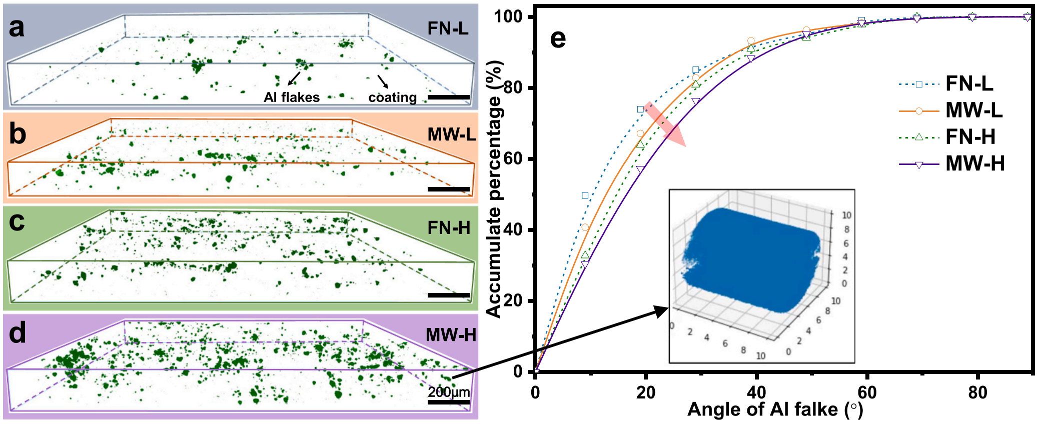

Fig. 7. Orientation of Al flakes in films; a-d) micro-CT 3D images of Al flakes dispersed in the coating films; e) the accumulated percentage of the cute angles between Al flakes and the substrate calculated from the micro-CT images.

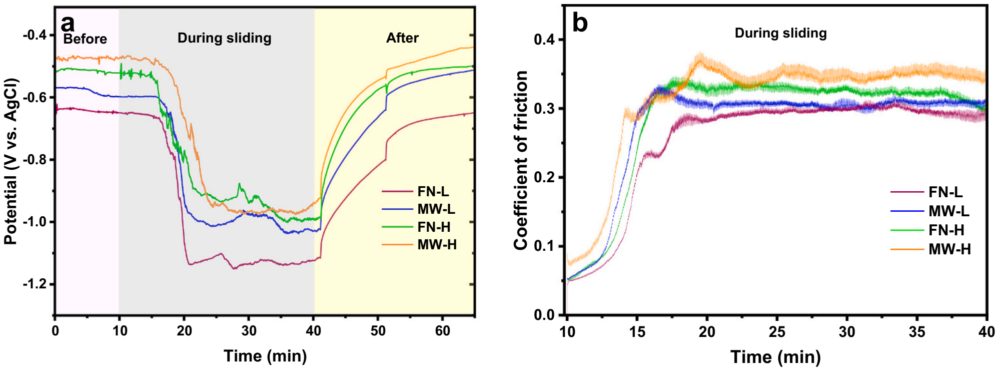

Fig. 8. Variation of OCP with time recorded before, during, and after sliding under different loads in 3.5 wt% NaCl solution with the COF values of prepared samples.

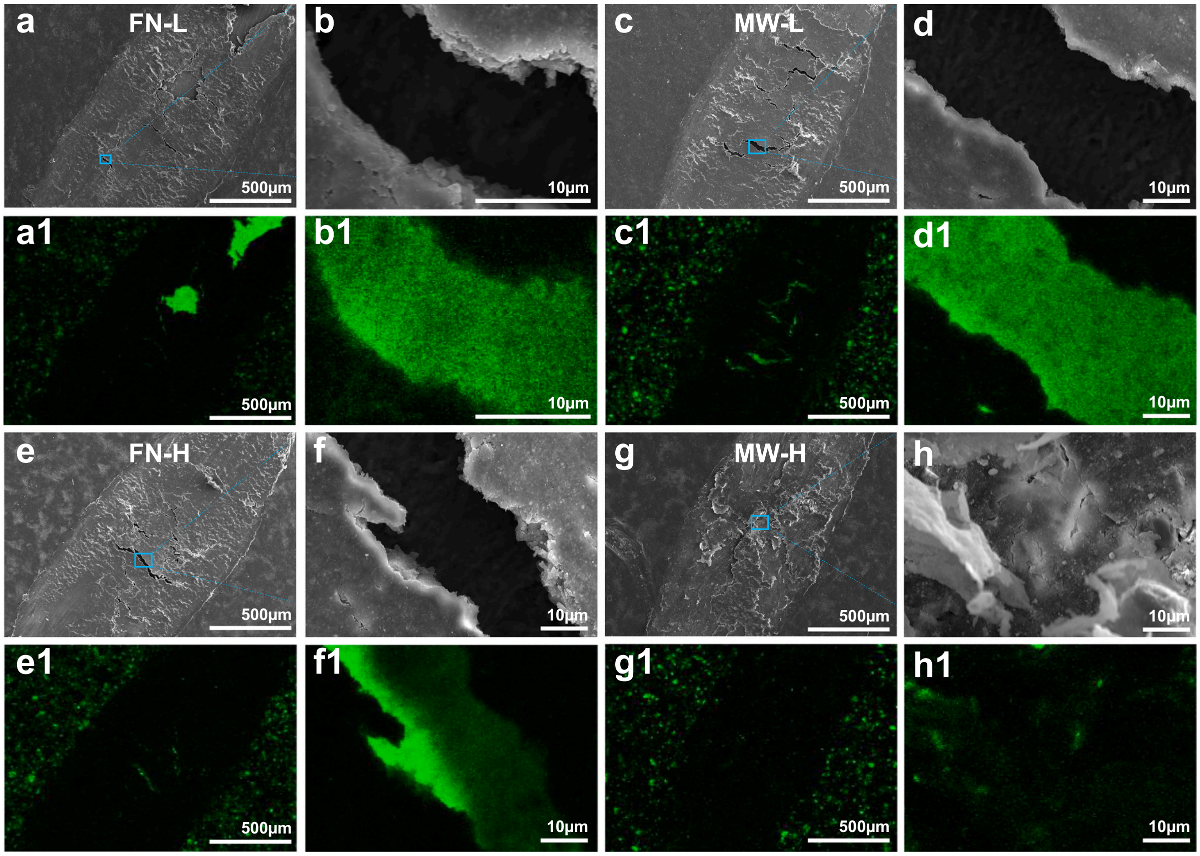

Fig. 9. SEM morphology and EDS elemental mapping of worn surfaces for prepared films under 10 N load after tribocorrosion. The green patterns exhibit the distribution of Al element. (For interpretation of the references to colour in this figure legend, the reader is referred to the web version of this article.)

significantly less severe than that of FN-L. Overall, the microwave-heated sample exhibited enhanced wear resistance with the original Al content of 2.33 wt%.

Fig. 9e,f and e1,f1 exhibited approximately five visible cracks in the FN-H film, which were less severe in comparison to MW-L. This results in a fluctuating and slightly higher OCP observed between 22 and 40 min. On the contrary, no discernible cracks that exposed the substrate were observed in the MW-H film after sliding, as shown in Fig. 9g,h and g1,h1. Both FN-H and MW-H exhibited uneven tracks in Fig. 10, with depths of 28 μm and 22 μm, respectively. It is evident that microwave-heated samples with a high content of Al flakes displayed improved resistance against wear and corrosion.

By integrating the aforementioned findings with the Al content outlined in Fig. 5, it is confirmed that the film containing a higher proportion of Al flakes exhibits superior resistance to wear and corrosion. Significantly, in cases where the original content of Al flake was identical, microwave-heated MPC displayed a higher deposited content Al content in comparison to its conventional friction-based counterpart, as schematized in Fig. 11a and b, because of a more significant number of bondings between the base coating particles and Al flakes. Upon immersion of the samples in a NaCl solution, the presence of Al flakes in the coating impeded the infiltration of the solution through pores [66]. The elevated quantity of Al flakes within the coating yielded more pronounced physical impedance, resulting in a higher OCP, as illustrated in Fig. 8a. The inclusion of more Al flakes enhanced the wear resistance of the MPC coating, alleviated damage and reduced the depths of the tracks formed during sliding, as schematized in Fig. 11c and d.

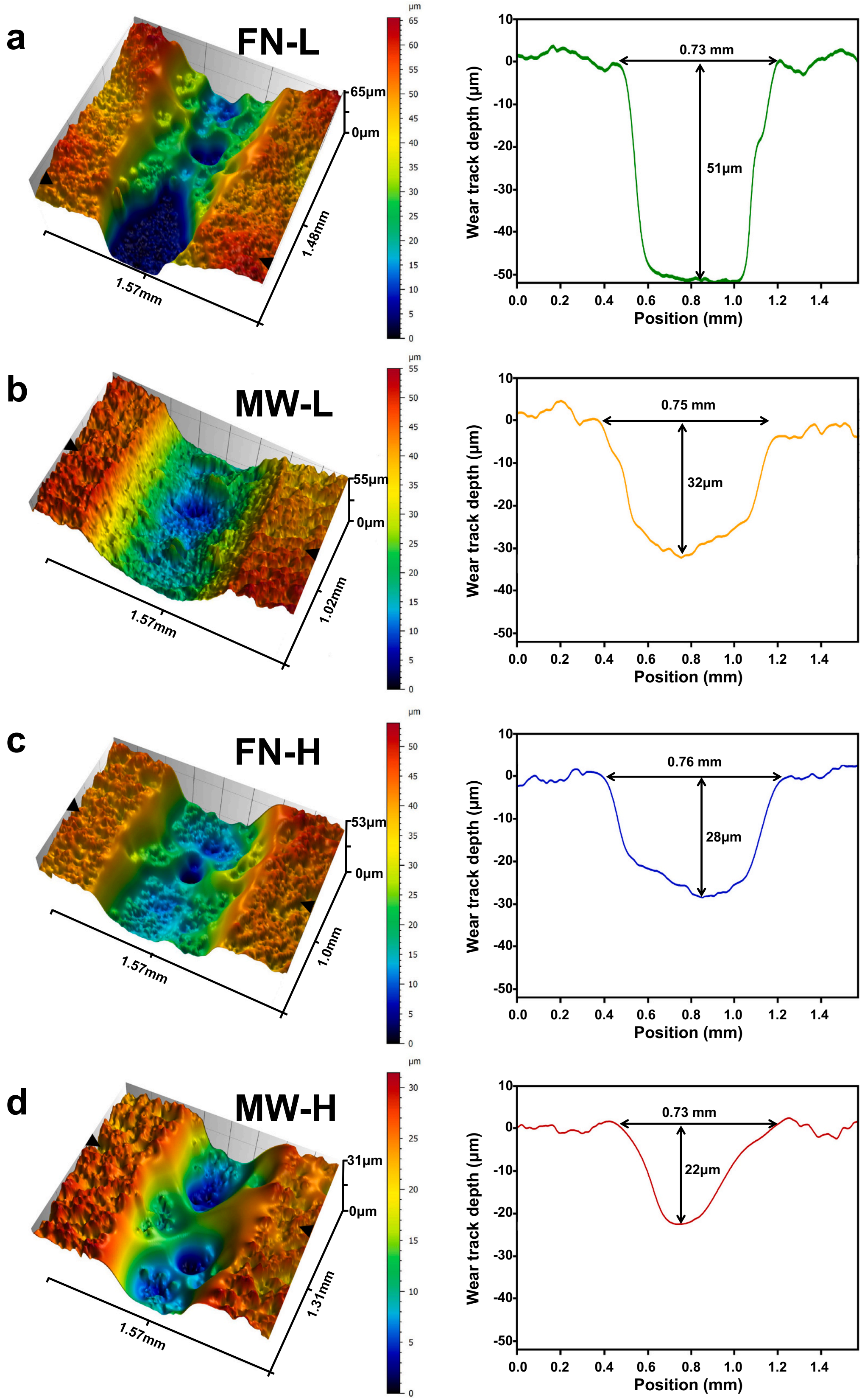

Fig. 10. 3D morphology of the wear tracks and extracted profiles (between the two black triangles) for the prepared coatings under 10 N load after tribocorrosion tests.

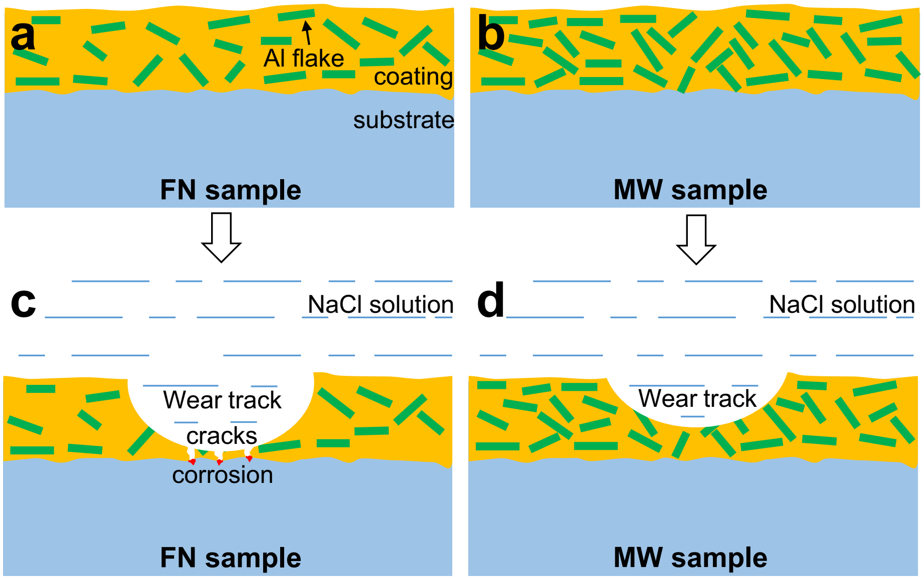

Fig. 11. Schematic draws of the suggested tribocorrosion mechanisms for friction-heated (FN) (a, c) and microwave-heated (MW) (b, d) samples when the original Al content is high.

3.4. Properties of films

Table 2 presents the comparison of the physical and chemical properties of the prepared films. The results indicate no significant difference in hardness and adhesion among the films, except for the film of MW-H. This film exhibits one grade higher hardness than the others, but one grade lower adhesion. The higher content of Al flakes (as given in Fig. 5) in the film is the primary reason for the changes observed. While the high Al content enhances the hardness by providing metallic properties, it also reduces flexibility by hindering the interpenetrating resinous network. Due to the extension property of aluminum being inferior to the polyester resin, the direct impact resistance of the films decreased and slight crackings were seen (Fig. S4) after bending when the Al content increased. The four samples passed the acid, hydrolytic, solvent and stain resistance tests (Figs. S6-S8). The colors of the four samples changed after alkali resistance tests at the tested areas (Fig. S5). The primary factor contributing to this outcome is the deliberate selection of Al flakes with low alkali resistance, a selection strategically advantageous for the analysis of gas volume through NaOH (Eq. (5)).

The present study displays visual comparisons of the metallic effect on car models, as depicted in Fig. 12. To ensure a stable metallic effect, commercial MPC typically contains less than 2.5 wt% of Al flake, which represents the highest content available. Thus, in this study, the FN-L sample containing 2.33 wt% Al flake was selected to represent the maximum level of metallic effect that commercial products can attain (Fig. 12b). However, the samples prepared through microwave heating bonding exhibited stable and extensive metallic effect even at an Al flake content of approximately 5 wt%, according to prior findings. The final finish, derived from the MW-H sample presented in Fig. 12c, presented a more pronounced metallic effect when compared to the commercial product. Notably, the light strip on the hood disappeared due to the high multi-angle reflection of the metallic effect. It is evident that the stable microwave-heated sample demonstrates a considerably more intense metallic effect than the commercial product.

Table 2
The performances of friction and microwave bonded films with low and high addition of Al flakes.

	FN-L	MW-L	FN-H	MW-H
Hardness	HB	HB	HB	F
Adhesion	5B	5B	5B	4B
Direct impact	343 N·cm	323 N·cm	177 N·cm	128 N·cm
Bending	No cracking	No cracking	Slight cracking	Slight cracking
Acid resistance	Pass	Pass	Pass	Pass
Alkali resistance	Changed	Changed	Changed	Changed
Hydrolytic stability	Pass	Pass	Pass	Pass
Solvent resistance	Pass	Pass	Pass	Pass
Stain resistance	Pass	Pass	Pass	Pass

4. Conclusions

A novel approach for manufacturing metallic powder coatings (MPCs) that have a stable and intensified metallic effect as well as improved tribocorrosion resistance was investigated and discussed in this study. Compared to the current friction-based technique, the microwave-based method obtained much higher heating rates and enhanced bondings between Al flakes and base coating particles, as well as acquired a more stable and stronger metallic effect. The selective heating of microwave comes from the interface polarization and exhibited overall superiority over friction heating in producing metallic powder coatings.

When the original Al content remained constant, the utilization of microwave heating led to an elevation in the Al content within the coating, which gave the coating a higher corrosion resistance due to less disrupted coatings and a higher coefficient of friction due to more Al flakes. The higher Al content also enhanced the protection of the coating and reduced the track depths and film damage after the sliding test. In conclusion, the microwave-based bonding method shows great potential for efficiently preparing stable and intensified MPCs with enhanced corrosion and wear resistance.

CRediT authorship contribution statement

Wei Liu: Writing – original draft, Visualization, Validation, Software, Methodology, Investigation, Formal analysis, Data curation. **Marshall Yang:** Validation, Software, Formal analysis. **Xinping Zhu:** Resources. **Yufu Wei:** Project administration. **Yolanda Hedberg:** Writing – review & editing, Funding acquisition. **Hui Zhang:** Writing – review & editing, Supervision, Funding acquisition, Conceptualization. **Jesse Zhu:** Writing – review & editing, Supervision, Funding acquisition.

Fig. 12. Stainless car models: a) uncoated; b) coated with commercial MPC with 2.33 wt% Al flake; c) coated with microwave-based bonded sample with 4.94 wt% Al flake.

Declaration of competing interest

The authors declare that they have no known competing financial interests or personal relationships that could have appeared to influence the work reported in this paper.

Data availability

Data will be made available on request.

Acknowledgement

This research was funded in part by The Natural Sciences and Engineering Research Council of Canada (NSERC) Discovery Grants, No. RGPIN-2018-06256, DGDND-2021-03997 and RGPIN-2021-03997; NSERC Research Tools and Instruments grants program (RTI), No. RTI-2021-00452; The Canada Research Chairs Program, No. CRC-2019-00425; the Wolfe-Western Fellowship, grant number 2020; The Social Sciences and Humanities Research Council (SSHRC), The New Frontiers in Research Fund (NFRF), Transformation, No. NFRFT-2020-00573; the Foshan Science and Technology Bureau (Foshan Science and Technology Innovation Project 1920001000150-08). The authors would like to express gratitude to Guangdong Huajiang Powder Technology Co., Ltd., Guangdong, China (www.rivers-coatings.com) for its contribution to providing a facility for experimentation, and to the specialists at Surface Science Western and the Department of Chemistry, Western University (The University of Western Ontario) for training and technical support. The authors would like to thank the Department of Chemical and Biochemical Engineering, Western University for providing COMSOL. The authors are grateful to Dr. Jinbao Huang, Zhengzhou Research Institute, Harbin Institute of Technology, for help with the micro-CT technique.

Appendix A. Supplementary data

Supplementary data to this article can be found online at https://doi.org/10.1016/j.porgcoat.2024.108218.

References

[1] A.B. Asha, A. Ounkaew, Y.-Y. Peng, M.R. Gholipour, K. Ishihara, Y. Liu, R. Narain, Bioinspired antifouling and antibacterial polymer coating with intrinsic self-healing property, Biomater. Sci. 11 (1) (2023) 128–139.
[2] W. Zhao, X. Han, Y. Lu, Z. Zhang, Q. Zhang, P. Peng, H. Wu, Fabrication of mechanically robust urushiol-based polymer coatings with excellent self-healing property and hydrophobicity, Prog. Org. Coat. 174 (2023) 107237, https://doi.org/10.1016/j.porgcoat.2022.107237.
[3] A. Dixit, A. Sabnis, D. Balgude, S. Kale, A. Gada, B. Kudu, K. Mehta, S. Kasar, D. Handa, R. Mehta, et al., Synthesis and characterization of citric acid and itaconic acid-based two-pack polyurethane antimicrobial coatings, Polym. Bull. 80 (2) (2023) 2187–2216.
[4] A. Dixit, A. Sabnis, A. Shetty, Antimicrobial edible films and coatings based on n, o-carboxymethyl chitosan incorporated with ferula asafoetida (hing) and adhatoda vasica (adulsa) extract, Adv. Mater. Process. Technol. 8 (3) (2022) 2699–2715.
[5] M.K. Gunde, M. Kunaver, A. Hrovat, U. Cvelbar, Bonding process efficiency and Al-flake orientation during the curing of powder coatings, Prog. Org. Coat. 54 (2) (2005) 113–119.
[6] J. Huang, M. Yang, W. Zhu, K. Tang, H. Zhang, J. Chen, J.J. Noël, I. Barker, H. Zhang, J. Zhu, Extrusion-free fabrication of zinc-rich powder coatings: press bondingc, Chem. Eng. J. 442 (2022) 135925.
[7] J. Mårdalen, J.E. Lein, H. Bolm, M. Hallenstvet, V. Rekowski, Time and cost effective methods for testing chemical resistance of aluminium metallic pigmented powder coatings, Prog. Org. Coat. 63 (1) (2008) 49–54.
[8] M. Barletta, D. Bellisario, Effects of ir pre-curing conditions on wear resistance of metal flake powder coatings, Prog. Org. Coat. 70 (4) (2011) 273–286.
[9] A. Iwakoshi, T. Nanke, T. Kobayashi, Coating materials containing gold nanoparticles, Gold Bull. 38 (2005) 107–112.
[10] M.K. Gunde, M. Kunaver, M. Mozetic, P. Pelicon, J. Simcic, M. Budnar, M. Bele, Microstructure analysis of metal-effect coatings, Surf. Coat. Int. B: Coat. Trans. 85 (2) (2002) 115–121.
[11] W. Liu, H. Zhang, Y. Shao, H. Zhang, J. Zhu, Preparation of aluminium metallic pigmented powder coatings with high color stability using a novel method: microwave bonding, Prog. Org. Coat. 147 (2020) 105787.
[12] W. Liu, J. Fu, H. Zhang, Y. Shao, H. Zhang, J. Zhu, Cold bonding method for metallic powder coatings, Materials 11 (11) (2018) 2086.
[13] L. Prendi, P. Henshaw, E.K. Tam, Automotive coatings with improved environmental performance, Int. J. Environ. Stud. 63 (4) (2006) 463–471.
[14] D. Czachor-Jadacka, B. Pilch-Pitera, Progress in development of uv curable powder coatings, Prog. Org. Coat. 158 (2021) 106355, https://doi.org/10.1016/j.porgcoat.2021.106355.
[15] X. Zhong, L. Lv, H. Hu, X. Jiang, H. Fu, Bio-based coatings with liquid repellency for various applications, Chem. Eng. J. 382 (2020) 123042.
[16] E. Vermoesen, E. Cordeels, D. Schaubroeck, G. Brosens, S. Bodé, P. Boeckx, S. Van Vlierberghe, Photo-crosslinkable biodegradable polymer coating to control fertilizer release, Eur. Polym. J. 186 (2023) 111835, https://doi.org/10.1016/j.eurpolymj.2023.111835.
[17] A. Kathuria, S. Zhang, Sustainable and repulpable barrier coatings for fiber-based materials for food packaging: a review, Front. Mater. 9 (2022) 929501.
[18] B. Biegańska, M. Zubielewicz, E. Śmieszek, Anticorrosive water-borne paints, Prog. Org. Coat. 15 (1) (1987) 33–56.
[19] M.J. Nine, S. Kabiri, T.T. Tung, D.N. Tran, D. Losic, Electrostatic powder coatings of pristine graphene: a new approach for coating of granular and fibril substrates, Appl. Surf. Sci. 441 (2018) 187–193.
[20] J. Cui, Y. Shao, H. Zhang, H. Zhang, J. Zhu, Development of a novel silver ions-nanosilver complementary composite as antimicrobial additive for powder coating, Chem. Eng. J. 420 (2021) 127633.
[21] W. Liu, H. Zhang, Y. Shao, H. Zhang, J. Zhu, Produce various powder coated surfaces with stable metal shine via microwave energy, Prog. Org. Coat. 154 (2021) 106199.
[22] J. Fu, M. Krantz, H. Zhang, J. Zhu, H. Kuo, Y.M. Wang, K. Lis, Investigation of the recyclability of powder coatings, Powder Technol. 211 (1) (2011) 38–45.
[23] S. Mahajan, A.V. Mayur, N.M. Pratiksha, V.P. Sneha, Review on automotive body coating process, Int. J. Eng. Manag. Res. 9 (2) (2019) 103–106.
[24] A.S.H. Makhlouf, Y. Gajarla, Advances in smart coatings for magnesium alloys and their applications in industry, in: Advances in Smart Coatings and Thin Films for Future Industrial and Biomedical Engineering Applications, Elsevier, 2020, pp. 245–261.
[25] Y. Takano, Metallic pigment and coating material containing the same, US Patent App. 11/792,861 (Apr. 3 2008).
[26] G. Wu, D. Yu, Preparation and characterization of a new low infrared-emissivity coating based on modified aluminum, Prog. Org. Coat. 76 (1) (2013) 107–112.
[27] K. Endoh, A. Nagahara, Y. Hisaeda, T. Ueyama, Bonding material using metal nanoparticles coated with c6-c8 fatty acids, and bonding method, US Patent 8,858,700 (Oct. 14 2014).
[28] S. Nain, R. Singh, S. Ravichandran, Importance of microwave heating in organic synthesis, Adv. J. Chem. Sect. A 2 (2) (2019) 94–104.

[29] V. Singh, P. Kumar, R. Sanghi, Use of microwave irradiation in the grafting modification of the polysaccharides–a review, Prog. Polym. Sci. 37 (2) (2012) 340–364.

[30] A. Kokel, C. Schäfer, B. Török, Application of microwave-assisted heterogeneous catalysis in sustainable synthesis design, Green Chem. 19 (16) (2017) 3729–3751.

[31] S. Putz, A. Angerer, D.O. Krimer, R. Glattauer, W.J. Munro, S. Rotter, J. Schmiedmayer, J. Majer, Spectral hole burning and its application in microwave photonics, Nat. Photonics 11 (1) (2017) 36.

[32] I. Das, A. Arora, Alternate microwave and convective hot air application for rapid mushroom drying, J. Food Eng. 223 (2018) 208–219.

[33] A. Raveendran, M.T. Sebastian, S. Raman, Applications of microwave materials: a review, J. Electron. Mater. 48 (5) (2019) 2601–2634.

[34] R.R. Mishra, A.K. Sharma, Microwave–material interaction phenomena: heating mechanisms, challenges and opportunities in material processing, Compos. Part A Appl. Sci. Manuf. 81 (2016) 78–97.

[35] A. Metaxas, R.J. Meredith, Industrial Microwave Heating, IET, 1983.

[36] J. K. Mistry, J. P. Frick, J. Petersen, Microwave bonding for coating compositions, US Patent 15,463,131 (Jul. 6 2017).

[37] D. Pletcher, Z.-Q. Tian, D. Williams, Tribocorrosion, in: Developments in Electrochemistry: Science Inspired by Martin Fleischmann, John Wiley & Sons, 2014, pp. 281–294.

[38] L.K. Prasad, J.W. McGinity, R.O. Williams III, Electrostatic powder coating: principles and pharmaceutical applications, Int. J. Pharm. 505 (1–2) (2016) 289–302.

[39] X. Meng, J.J. Zhu, H. Zhang, Influences of different powders on the characteristics of particle charging and deposition in powder coating processes, J. Electrost. 67 (4) (2009) 663–671.

[40] W. Liu, H. Zhang, Y. Shao, X. Zhu, Y. Wei, H. Zhang, J. Zhu, Applying microwave energy to fabricate powder coatings with strong and stable metal shine, Prog. Org. Coat. 149 (2020) 105929.

[41] T. Hanai, Dielectric theory on the interfacial polarization for two-phase mixtures, Bull. Inst. Chem. Res. Kyoto Univ. 39 (6) (1962) 341–367.

[42] W. Chi, S. Sampath, H. Wang, Ambient and high-temperature thermal conductivity of thermal sprayed coatings, J. Therm. Spray Technol. 15 (2006) 773–778.

[43] L.-F. Chen, C. Ong, C. Neo, V. Varadan, V.K. Varadan, Microwave Electronics: Measurement and Materials Characterization, John Wiley & Sons, 2004.

[44] H.G. Kim, et al., Dielectric cure monitoring for glass/polyester prepreg composites, Compos. Struct. 57 (1–4) (2002) 91–99.

[45] K.S. Kiew, S. Hamdan, M.R. Rahman, Comparative study of dielectric properties of chicken feather/kenaf fiber reinforced unsaturated polyester composites, BioResources 8 (2) (2013) 1591–1603.

[46] K. Wagner, Explanation of dielectric polarization processes on the basis of maxwellian concepts, Arch. Electrotech. 2 (1914) 371–387.

[47] R. Sillars, The properties of a dielectric containing semiconducting particles of various shapes, J Inst. Electr. Eng. 80 (484) (1937) 378–394.

[48] M. Yoshizumi, Electroconductive powder and process for production thereof, US Patent 4,452,830 (Jun. 5 1984).

[49] D. Goldwater, B. Stickler, L. Martinetz, T.E. Northup, K. Hornberger, J. Millen, Levitated electromechanics: all-electrical cooling of charged nano-and micro-particles, Quantum Sci. Technol. 4 (2) (2018) 024003.

[50] Z.-M. Dang, T. Zhou, S.-H. Yao, J.-K. Yuan, J.-W. Zha, H.-T. Song, J.-Y. Li, Q. Chen, W.-T. Yang, J. Bai, Advanced calcium copper titanate/polyimide functional hybrid films with high dielectric permittivity, Adv. Mater. 21 (20) (2009) 2077–2082.

[51] J. D. Christie, W. C. Howard, Bonded metal hydroxide-organic composite polymer films on particulate substrates, US Patent 6,245,323 (Jun. 12 2001).

[52] D. Suh, O. Park, K. Yoon, The properties of unsaturated polyester based on the glycolyzed poly (ethylene terephthalate) with various glycol compositions, Polymer 41 (2) (2000) 461–466.

[53] E. Sanchez, C. Zavaglia, M. Felisberti, Unsaturated polyester resins: influence of the styrene concentration on the miscibility and mechanical properties, Polymer 41 (2) (2000) 765–769.

[54] K. Bansal, J.A. Pojman, D. Webster, M. Quadir, Frontal polymerization of a thin film on a wood substrate, ACS Macro Lett. 9 (2) (2020) 169–173.

[55] K. Breuer, M. Stommel, W. Korte, Analysis and evaluation of fiber orientation reconstruction methods, J. Compos. Sci. 3 (3) (2019) 67.

[56] B. Zhang, J. Wang, F. Yan, Load-dependent tribocorrosion behaviour of nickel-aluminium bronze in artificial seawater, Corros. Sci. 131 (2018) 252–263.

[57] J. Ju, R. Zan, Z. Shen, C. Wang, P. Peng, J. Wang, B. Sun, B. Xiao, Q. Li, S. Liu, T. Yang, Remarkable bioactivity, bio-tribological, antibacterial, and anti-corrosion properties in a Ti-6Al-4V-xCu alloy by laser powder bed fusion for superior biomedical implant applications, Chem. Eng. J. 471 (2023) 144656.

[58] S. Khireche, D. Boughrara, A. Kadri, L. Hamadou, N. Benbrahim, Corrosion mechanism of Al, Al–Zn and Al–Zn–Sn alloys in 3wt.% NaCl solution, Corros. Sci. 87 (2014) 504–516.

[59] T. Cheng, H. Huang, G. Huang, Galvanic corrosion behavior between ADC12 aluminum alloy and copper in 3.5 wt% NaCl solution, J. Electroanal. Chem. 927 (2022) 116984.

[60] J.R. Nowers, B. Narasimhan, The effect of interpenetrating polymer network formation on polymerization kinetics in an epoxy-acrylate system, Polymer 47 (4) (2006) 1108–1118.

[61] S. Liu, G. Li, Y. Qi, Z. Peng, Y. Ye, J. Liang, Corrosion and tribocorrosion resistance of MAO-based composite coating on AZ31 magnesium alloy, J. Magnes. Alloys 10 (12) (2022) 3406–3417.

[62] S. Liu, Y. Jing, T. Zhang, J. Zhang, F. Xu, Q. Song, Q. Ye, S. Liu, W. Liu, Excellent tribological and anti-corrosion performances enabled by novel hollow graphite carbon nanosphere with controlled release of corrosion inhibitor, Chem. Eng. J. 412 (2021) 128648.

[63] R. Jamaati, M. Toroghinejad, J. Szpunar, D. Li, Tribocorrosion behaviour of Al/Al_2O_3 mmc produced by ARB process, Tribol. Mater. Surf. Interfaces 5 (1) (2011) 10–15.

[64] M. Kalaee, S. Akhlaghi, A. Nouri, S. Mazinani, M. Mortezaei, M. Afshari, D. Mostafanezhad, A. Allahbakhsh, H.A. Dehaghi, A. Amirsadri, et al., Effect of nano-sized calcium carbonate on cure kinetics and properties of polyester/epoxy blend powder coatings, Prog. Org. Coat. 71 (2) (2011) 173–180.

[65] S. Narayan, A. Rajeshkannan, Hardness, tensile and impact behaviour of hot forged aluminium metal matrix composites, J. Mater. Res. Technol. 6 (3) (2017) 213–219.

[66] S. Yang, J. Huang, J. Chen, J.J. Noël, I. Barker, J.D. Henderson, P. He, H. Zhang, H. Zhang, J. Zhu, A comparative study on the anti-corrosive performance of zinc phosphate in powder coatings, Coatings 12 (2) (2022) 217.